SCATTERING-BASED DECOMPOSITION OF SENSITIVITY KERNELS FOR FULL WAVEFORM INVERSION – PART 2: PERTURBATION ESTIMATES WITH ADJOINT KERNELS

D. Macedo, I. Vasconcelos, and J. Schleicher

email: *dlmacbr@gmail.com*

keywords: *Full waveform inversion, Scattering theory, multiscale decomposition, multiple scattering*

ABSTRACT

Migration methods based on the wave equation require refined earth models. A wave-equation based tool for Earth modelling is full waveform inversion (FWI). While in principle capable of handling all aspects of wave propagation contained in the data, including full nonlinearity, in practice nonlinear gradient-based FWI is limited due to its notorious sensitivity to the choice of the starting model. To help addressing model-convergence issues in FWI, we study a decomposition based on scattering theory that allows to break the acoustic-wavefield sensitivity kernels with respect to model parameters into background and singular parts. Estimates for both background perturbation and/or singular-part perturbation obtained with the subkernels' adjoints are components of the estimate obtained with the full kernel's adjoint. Our numerical experiments have shown the feasibility of our main claim: the decomposition into subkernels allow to backproject only the scattered-wavefield residuals only so as to obtain reasonable background-model perturbation estimates. In an experiment with restricted acquisition geometry (reflection data, narrow offset), the multiple-scattering subkernels take advantage of medium self-illumination provided by the scattered wavefields.

INTRODUCTION

In the last decade, as the industry has been facing geologically more complex areas, new migration methods have been developed, because older, ray-based techniques were not sufficient to provide the high-quality images required for successful hydrocarbon exploration. Those new methods, like wave-equation migration or reverse-time migration, require more and more refined earth models. However, even though migration has advanced quickly with the raise of available computer power, standard techniques for constructing these models are still mostly ray-based. Recently, one tool for Earth modelling based on the two-way wave-equation has been studied and developed by many authors: full waveform inversion (FWI) (see, e.g. Vigh et al., 2009; Virieux and Operto, 2009).

While in principle capable of handling all aspects of wave propagation contained in the data, including full nonlinearity, in practice nonlinear gradient-based FWI is limited due to its notorious sensitivity to the choice of the starting model. This is so because for short-offset acquisition of reflection data, the seismic wavefield is rather insensitive to high/intermediate wavelengths.

To help addressing model convergence issues in FWI, we study a decomposition based on scattering theory that allows to break the acoustic-wavefield sensitivity kernels (SKs) with respect to model parameters into background and singular parts. In last year's WIT report, Macedo et al. (2011) were able to demonstrate that the *forward* decomposition is successful in bringing out subkernels that unravelled different levels of non-linearity with respect to data and model. This, in turn, could be translated into different levels of interaction between non-, single-, and multiple-scattered information that otherwise would be hidden in the full-wavefield sensitivity kernels. Moreover, Macedo et al. (2011) predicted that part of the

answer to the problem of lacking low-frequency information on the model should lie in utilizing scattered wavefields, because these travel through the medium long enough to carry this information (see also Snieder et al., 2002).

In this work, we report on the progress of our study. In particular, we show numerical results of using those subkernels to backproject the *scattered residual* only into model space and obtain model perturbation estimates.

SCATTERING-BASED SENSITIVITY KERNELS

The decomposition of the full wavefield into a reference and scattered wavefields (Macedo et al., 2011, equations 2 to 5) leads to a decomposition of the full wavefield perturbation (residual) into two wavefields residuals. In the frequency domain, we can write

$$\begin{bmatrix} \widehat{\delta p}_0 \\ \widehat{\delta p}_s \end{bmatrix} = \begin{bmatrix} U & V & 0 & 0 \\ U_B & V_B & U_S & V_S \end{bmatrix} \begin{bmatrix} \delta K_B \\ \delta \rho_B \\ \delta K_S \\ \delta \rho_S \end{bmatrix}. \tag{1}$$

Here, δp_0 and δp_s are the reference and scattered-wavefield residuals, respectively, and the hat stands for the Fourier transform in time. Moreover, δK_B and $\delta \rho_B$ are the perturbations of the background model parameters, δK_S and $\delta \rho_S$ perturbations on the singular model parameters. U and V are the SKs of the reference wave field with respect to the background parts of the bulk modulus and density; U_B and V_B are the SKs of the scattered wavefield with respect to the background parts of the bulk modulus and density; and U_S and V_S are the SKs of the scattered wavefield with respect to the singular parts of the bulk modulus and density, respectively.

Equation (1) represents two time-domain integral equations, the first of which takes the form

$$\delta p_0(x,t;x_s) = -\int_{\mathbb{V}} d^3x'\, G_0(x,t;x') * \delta\mathcal{L}^B\left[p_0(x',t;x_s)\right]. \tag{2}$$

where $\delta\mathcal{L}^B$ is the background secondary potential, and p_0 and G_0 are the wavefield and the Green's function in the unperturbed background medium (Macedo et al., 2011, equation 17).

Likewise, the second equation of system (1) takes the integral form of:

$$\begin{aligned}
\delta p_s(x_g,t;x_s) = \sum_{i=1}^{n=8} \delta p_{s,i}(x_g,t;x_s) = \\
&- \int_{\mathbb{V}} d^3x'\, G_s(x',t;x_g) * \mathcal{V}\left[\delta p_0(x',t;x_s)\right] - \int_{\mathbb{V}} d^3x'\, G_0(x',t;x_g) * \mathcal{V}\left[\delta p_0(x',t;x_s)\right] \\
&- \int_{\mathbb{V}} d^3x'\, G_s(x',t;x_g) * \delta\mathcal{L}\left[p_0(x',t;x_s)\right] - \int_{\mathbb{V}} d^3x'\, G_0(x',t;x_g) * \delta\mathcal{L}\left[p_0(x',t;x_s)\right] \\
&- \int_{\mathbb{V}} d^3x'\, G_s(x',t;x_g) * \delta\mathcal{L}\left[p_s(x',t;x_s)\right] - \int_{\mathbb{V}} d^3x'\, G_0(x',t;x_g) * \delta\mathcal{L}\left[p_s(x',t;x_s)\right] \\
&+ \int_{\mathbb{V}} d^3x'\, G_s(x',t;x_g) * \delta\mathcal{L}^B\left[p_0(x',t;x_s)\right] + \int_{\mathbb{V}} d^3x'\, G_0(x',t;x_g) * \delta\mathcal{L}^B\left[p_0(x',t;x_s)\right],
\end{aligned} \tag{3}$$

where $\mathcal{V}$ is the scattering potential, $\delta\mathcal{L}$ is the full secondary potential, and p_s and G_s are the scattered wavefield and Green's function in the unperturbed medium (Macedo et al., 2011, equation 7).

Kernels' physical interpretation: naming the terms

As we have seen in Figure 1 of Macedo et al. (2011), each of the terms of equation (3) reveals a different level of interaction between single and multiple-scattered information within data. In the standard formulation (Tarantola, 1984), these levels are hidden in the sensitivity kernel for the full wavefield. We are going to rename the terms based on their interaction level.

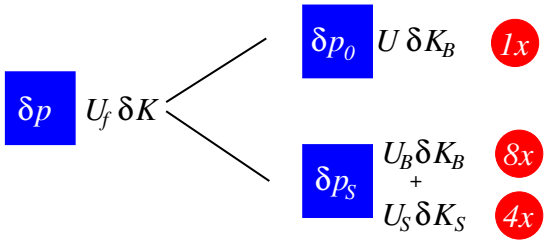

Figure 1: Subkernels obtained from the decomposition considering no perturbation in density.

Before we can do this, we must further decompose each term from $\delta p_{s,3}$ to $\delta p_{s,6}$, because the secondary potential $\delta\mathcal{L} = \delta\mathcal{L}^{\mathcal{B}} + \delta\mathcal{L}^{\mathcal{S}}$ possesses two parts depending on the perturbations of the smooth background ($\delta\mathcal{L}^{\mathcal{B}} \neq \delta\mathcal{L}^{B}$) and singular part ($\delta\mathcal{L}^{\mathcal{S}}$) of the model. As an example, let us take the third contribution $\delta p_{s,3}$. It actually consists of four contributions

$$\delta p_{s,3}(x_g,t;x_s) = \delta p^{K}_{s,3B}(x_g,t;x_s) + \delta p^{K}_{s,3S}(x_g,t;x_s) + \delta p^{\rho}_{s,3B}(x_g,t;x_s) + \delta p^{\rho}_{s,3S}(x_g,t;x_s)\,, \qquad (4)$$

corresponding to the four perturbations δK_B, δK_S, $\delta\rho_B$, and $\delta\rho_S$. The first of these contributions corresponds to the background bulk-modulus part of the full secondary potential and has the form

$$\delta p^{K}_{s,3B}(x_g,t;x_s) = -\left\{\int_{\mathbb{V}} d^3x' \left[\frac{1}{(K_B(x')+K_S(x'))^2}\, G_s(x',t;x_g) * \frac{\partial^2 p_0}{\partial t^2}(x',t;x_s)\right] \delta K_B(x')\,, \qquad (5)$$

and the others can be written correspondingly. The expression between the brackets describes the $\delta p_{s,3}$ part of the sensitivity kernel of the scattered-wavefield residual with respect to the smooth background of the bulk modulus, U_B of equation (1). Therefore, we will refer to it as $U_{B,3}$. Correspondingly, there are parts of the sensitivity kernel of the scattered-wavefield residual with respect to the singular part of the bulk modulus, U_S, and therefore called $U_{S,3}$, and to the smooth and singular parts of the density, $V_{B,3}$ and $V_{S,3}$. The terms $\delta p_{s,4}$, $\delta p_{s,5}$, and $\delta p_{s,6}$ can be decomposed analogously, giving rise to contributions to both sensitivity kernel. Note that in all four cases, the contribution to the background sensitivity kernel is equal to that to the singular-part sensitivity kernel, i.e., $U_{B,i} = U_{S,i}$ and $V_{B,i} = V_{S,i}$ ($i = 3,4,5,6$).

In this way, we arrive at thirteen subkernels (Figure 1) for each parameter of the full model, i.e., bulk modulus and density. These are one subkernel to evaluate the reference wavefield residual and twelve subkernels to evaluate the scattered-wavefield residual. Of the latter, eight depend on perturbations of the smooth part of the model and four depend on perturbations of the singular part. Therefore, equation (1) can be rewritten as

$$\begin{bmatrix} \widehat{\delta p}_0 \\ \widehat{\delta p}_s \end{bmatrix} = \begin{bmatrix} U & V & 0 & 0 \\ \sum_{i=1}^{n=8} U_{B,i} & \sum_{i=1}^{n=8} V_{B,i} & \sum_{i=3}^{n=6} U_{S,i} & \sum_{i=3}^{n=6} V_{S,i} \end{bmatrix} \begin{bmatrix} \delta K_B \\ \delta\rho_B \\ \delta K_S \\ \delta\rho_S \end{bmatrix}. \qquad (6)$$

In this notation, the subscripts of the contributions to the wavefield residuals are not very helpful to identify them. Thus, we relabel them based on their physical meaning as $\delta p_{s,\alpha\beta\gamma}$, where each of the three subscripts α, β, and γ stands for a physical action involved in the generation of the contribution. The first subscript, α, represents the wavefield that is responsible for the propagation of the contribution on the source side, the second subscript, β, stands for the potential operator causing the contribution, and the third subscript, γ, designates the wavefield that is responsible for the propagation of the contribution on the receiver side. The receiver-wavefield subscript γ is either 0 for the reference wavefield or s for the scattered wavefield. The source-wavefield subscript α can, in addition to 0 and s, also be b, representing the wavefield perturbation due to the background perturbation. The potential index β can take the values B, $\mathcal{B}$, $\mathcal{S}$ and $\mathcal{V}$, representing the background secondary potential, background part of full secondary potential, singular part of full secondary potential, and scattering potential, respectively. For instance, term $\delta p_{s,3B}$ of equation (5) becomes $\delta p_{s,0\mathcal{B}s}$. Figure 2 shows cartoons representing the physical interpretation of all

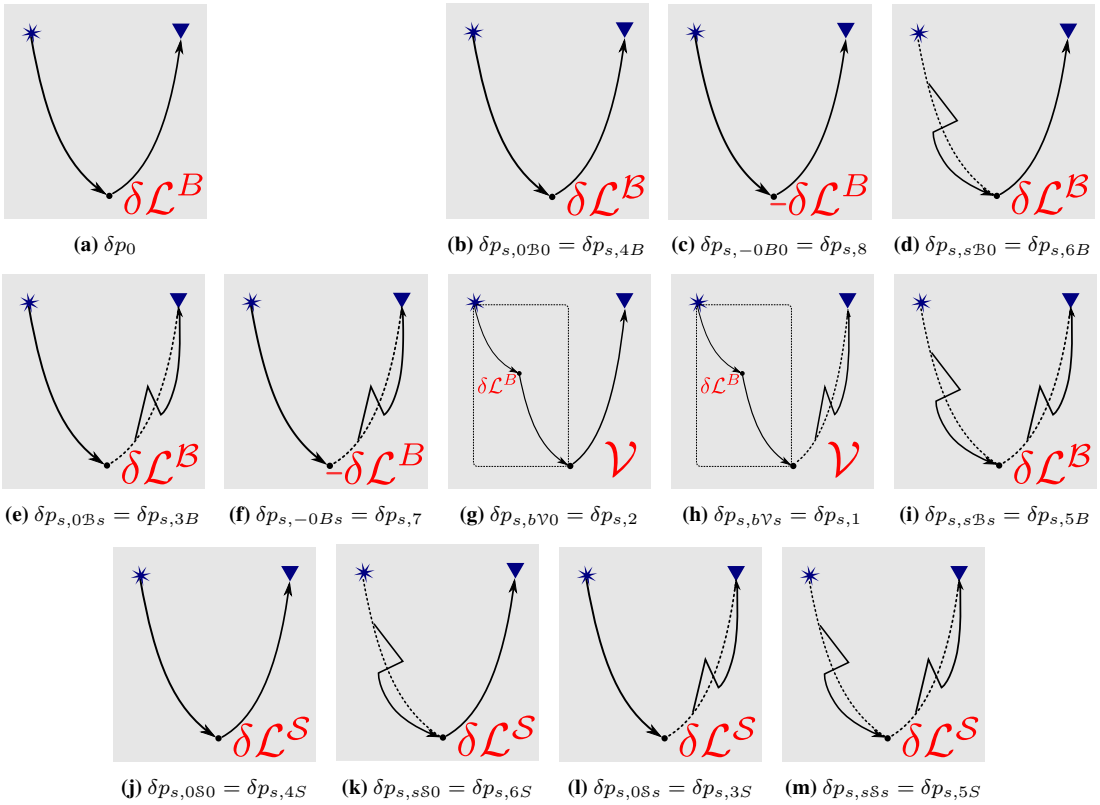

(a) δp_0 **(b)** $\delta p_{s,0\mathcal{B}0} = \delta p_{s,4B}$ **(c)** $\delta p_{s,-0B0} = \delta p_{s,8}$ **(d)** $\delta p_{s,s\mathcal{B}0} = \delta p_{s,6B}$

(e) $\delta p_{s,0\mathcal{B}s} = \delta p_{s,3B}$ **(f)** $\delta p_{s,-0Bs} = \delta p_{s,7}$ **(g)** $\delta p_{s,b\mathcal{V}0} = \delta p_{s,2}$ **(h)** $\delta p_{s,b\mathcal{V}s} = \delta p_{s,1}$ **(i)** $\delta p_{s,s\mathcal{B}s} = \delta p_{s,5B}$

(j) $\delta p_{s,0\mathcal{S}0} = \delta p_{s,4S}$ **(k)** $\delta p_{s,s\mathcal{S}0} = \delta p_{s,6S}$ **(l)** $\delta p_{s,0\mathcal{S}s} = \delta p_{s,3S}$ **(m)** $\delta p_{s,s\mathcal{S}s} = \delta p_{s,5S}$

Figure 2: Physical meaning of the subkernel contributions. Each one of the cartoons shows three elements: *source-side wavefield*; the *operator* applied to generate the secondary source; and the *receiver-side wavefield extrapolator*. Subcaptions indicate the new name and correspondence to the previous, numbered nomenclature.

thirteen bulk-modulus subkernels of equation (3). The subcaptions state the new name of each term and its old one in the previous, numbered nomenclature of equation (3). The subscripts of the contributions $U_{B,i}$, $U_{S,i}$, $V_{B,i}$, and $V_{S,i}$ to the sensitivity kernels are replaced accordingly.

In principle, we would need an additional index (for example, a superscript K or ρ) to indicate whether the contribution stems from a perturbation of the bulk modulus or density. Since in our numerical examples below, we restrict ourselves to bulk modulus perturbations, we will omit this additional index for the sake of simplicity.

BACKPROJECTING THE RESIDUALS INTO MODEL SPACE

The purpose of the residuals is to be used for model updating. This can be achieved by backprojecting the residuals into the model space with the help of the adjoint sensitivity kernels and using them to obtain estimates of the perturbation in the technique known as conjugate-gradient method (Mora, 1987; Tarantola, 1987; Crase et al., 1990).

Under the separation into background and singular components proposed here, estimates of background and singular model perturbations can be evaluated individually by backprojecting the residuals. The perturbation estimates are given by the adjoint to equation (6). Ignoring density perturbations for simplicity, they are obtained from

$$\begin{bmatrix} \delta K_B^{\text{est}} \\ \delta K_S^{\text{est}} \end{bmatrix} = \begin{bmatrix} \delta K_{B,0}^{\text{est}} + \sum_i \delta K_{B,i}^{\text{est}} \\ \sum_j \delta K_{S,j}^{\text{est}} \end{bmatrix} = \begin{bmatrix} U^\dagger & \sum_i U_{B,i}^\dagger \\ 0 & \sum_j U_{S,j}^\dagger \end{bmatrix} \begin{bmatrix} \widehat{\delta p}_0 \\ \widehat{\delta p}_s \end{bmatrix}. \tag{7}$$

with $i = 0\mathcal{B}0$, $0\mathcal{B}s$, $s\mathcal{B}0$, $s\mathcal{B}s$, $-0B0$, $-0Bs$, $b\mathcal{V}0$, $b\mathcal{V}s$, and $j = 0\mathcal{S}0$, $0\mathcal{S}s$, $s\mathcal{S}0$, and $s\mathcal{S}s$.

The physical meaning of these estimates is the same as the one given by Tarantola (1984). At each point x of the model, they are the cross-correlation between the direct wavefield from source with the (once or twice) backpropagated residual from the receivers. Explicitly, estimates $\delta K^{\text{est}}_{B,0\mathcal{B}s}$ and $\delta K^{\text{est}}_{B,b\mathcal{V}0}$ read

$$\delta K^{\text{est}}_{B,0\mathcal{B}s}(x) = \sum_s \sum_g \int d\omega \; \frac{-\omega^2}{K^2(x)} \overbrace{\widehat{p}^{\dagger}_0(x,\omega;x_s)}^{\text{direct wavefield}} \underbrace{\widehat{G}^{\dagger}_0(x,\omega;x_g)\widehat{\delta p}_s(x_g,\omega;x_s)}_{\text{back-propagation of } \widehat{\delta p}_s} \tag{8}$$

and

$$\delta K^{\text{est}}_{B,b\mathcal{V}0}(x) = \sum_s \sum_g \int d\omega \frac{-\omega^2}{K^2_B(x)} \overbrace{\widehat{p}^{\dagger}_0(x,\omega;x_s)}^{\text{direct wavefield}} \times$$

$$\int_{\mathbb{V}} d^3x' \underbrace{\widehat{G}^{\dagger}_0(x,\omega;x')}_{2^{\text{nd}} \text{ back-prop.}} \overbrace{\omega^2 \left(\frac{1}{K(x')} - \frac{1}{K_B(x')} \right)}^{\text{scattering potential at } x'} \underbrace{\widehat{G}^{\dagger}_0(x',\omega;x_g)\widehat{\delta p}_s(x_g,\omega;x_s)}_{1^{\text{st}} \text{ back-propagation of } \widehat{\delta p}_s \text{ to } x'} . \tag{9}$$

To get the explicit expressions of the other sensitivity kernels, one just needs to do the proper substitution of the wavefields and potentials.

Residual information leakage

Ideally, one could restrict the perturbation to a single part of the model. That's what we did in the experiments of last year's report (Macedo et al., 2011). However, backprojecting the residuals may lead to nonzero perturbation estimates for unperturbed parameters. We call this effect the *residual information leakage*. Generally speaking, when backprojected into model space, data residuals caused by a perturbation of the background model can leak to the estimates of the singular part of the model perturbation and vice-versa. From the above formulae, it is clear that there will be nonzero estimates for both δK_B and δK_S independently of whether only the scattered-wavefield residual or both, reference and scattered residuals are nonzero (there is no way to have only a nonzero reference-wavefield residual).

This matter is particularly important under the present decomposition. Since the sensitivity kernel contributions $U_{B,0\mathcal{B}0}$ and $U_{S,0\mathcal{S}0}$ are identical, so will be the estimates for both singular and background perturbations $\delta K^{\text{est}}_{B,0\mathcal{B}0}$ and $\delta K^{\text{est}}_{S,0\mathcal{S}0}$, when obtained from backprojecting residuals due to perturbation in the background (or singular) model only.

NUMERICAL EXPERIMENTS: BACKPROJECTING REFERENCE AND SCATTERED RESIDUALS

We have tested the above decomposition formulae in three numerical experiments using synthetic data. In all models tested, the density remained unperturbed at a constant value of 2200 kg/m^3. All experiments described in this report followed the same basic steps:

Model definition We defined an unperturbed model, modelled the full and reference wavefields, and extracted the scattered wavefield.

Model perturbation We introduced perturbations into the model, modelled the perturbed wavefields, and evaluated the true residuals.

True-residual backprojection We backpropagated the full, reference and scattered true residuals from a given source (once or twice) from a given receiver by the proper extrapolator.

Cross-correlation with direct wavefield We cross-correlated the backpropagated wavefield with the proper direct wavefield (full, reference, or scattered) from the corresponding source.

Stack We stacked the resulting wavefield over time (frequency), sources, and receivers.

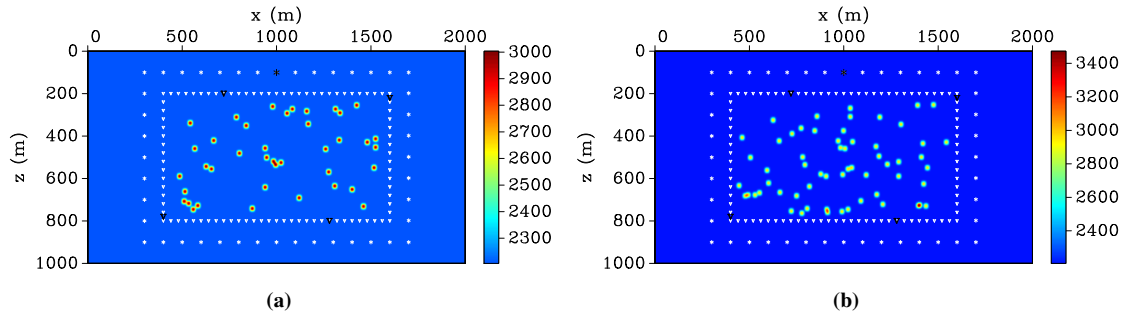

Figure 3: Unperturbed velocity models (velocity in m/s) containing (a) 40, (b) 60 randomly distributed scatterers, with constant background velocity (2205 m/s) and density (2200 kg/m^3). Four control receivers (black-triangles) are named clockwise from the top left as cr80, cr305, cr530, and cr755, respectively.

Figure 3 shows two unperturbed models used in the numerical experiments. Although velocity models are being displayed, the modeller used asked bulk modulus models as input, besides density. Both models seen in Figure 3 are obtained by the expression $v_p = \sqrt{K/\rho}$.

The model in Figure 3(a) was used in experiment 1 and the one shown in Figure 3(b) was used in experiments 2 and 3. In both, the background velocity has a constant value of 2205 m/s. The singular part of both models is composed of randomly distributed scatterers – 40 in (a) and 60 in (b). Each scatterer is represented as a bell-shaped perturbation with a maximum value of 798 m/s, obtained by horizontally and vertically smoothing a velocity perturbation in a square of 16 m width.

We performed non-simultaneous multiple-shots experiments. The sources and receiver positions are marked in Figure 3 by white and black stars and triangles, respectively. A staggered-grid time-domain finite-difference modeller was used to simulate wavefields with a 30 Hz Ricker signal as the source signature. The vertical grid spacing was 2 m; the horizontal one 4 m, and the time-marching step was 0.4 ms. The recorded wavefield was resampled to a 4 ms interval.

Together with the results, we employ the cartoons of Figure 2 to indicate which (sub)kernel is used to backproject the residuals and obtain the bulk modulus estimates. Each cartoon exhibits the kind of source-side wavefield (full, reference or scattered), the kind of receiver-side Green's function used to back-propagate the residual (some of them are built whit two backpropagations), and the differential operator applied before the cross-correlation between wavefields.

Experiment 1: Perturbing the scatterers' positions

In this experiment we only perturbed the singular part of the model by randomly modifying the scatterers' positions while leaving the background unchanged. The perturbations range from 0 to 24 m in the vertical and horizontal directions (see Figure 4). This yields perturbation of the scattered wavefield only – see equation (6).

Since in this case the full model perturbation δK is equal to the singular-part perturbation δK_S, we have $\delta p_0 = 0$ and the true full residual δp^{true} equals the true scattered residual δp_s^{true}, which is the residual we backprojected in this experiment. Therefore, according to equation (7), the bulk-modulus estimates are

$$\begin{bmatrix} \delta K_B^{\text{est}} \\ \delta K_S^{\text{est}} \end{bmatrix} = \begin{bmatrix} \sum_i U_{B,i}^{\dagger} \widehat{\delta p}_s^{\text{true}} \\ \sum_j U_{S,j}^{\dagger} \widehat{\delta p}_s^{\text{true}} \end{bmatrix}, \tag{10}$$

where the summation indices i and j take the values explained in connection with equation (7). Figure 5 compares δK_S^{est} to the full conventional bulk-modulus perturbation estimate δK^{est}. This figure points toward the success of the decomposition in this example. The summation of the four terms yielding δK_S^{est} (Figure 5a), leads exactly to the same result as the full bulk modulus perturbation estimate, δK^{est}, (Figure 5b). Here and in the following experiments, δK^{est} is always evaluated using the full wavefield Green's function (Macedo et al., 2011, equations 10 and 11).

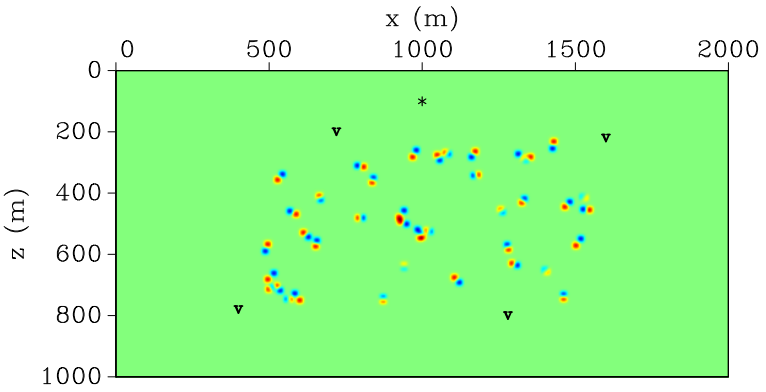

Figure 4: EXPERIMENT 1. Only the singular part of the model is perturbed, i.e., $\delta K_S \neq 0$. This is achieved by modifying the vertical and horizontal coordinates of the scatterers randomly within a given range. The cool (blue) spots show the unperturbed positions, while the hot (red) ones tell us the new positions. The intensity of the spots is related to the magnitude of the perturbation.

However, comparing Figures 4 and 5, one can see that the estimate is far from the true perturbation. The decomposition allows to dramatically improve the result (see Figure 6a). Actually, the single-scattering contribution $0\mathcal{S}0$ alone gives the best perturbation estimate. This is the term traditionally used when performing conjugate gradient FWI. This is not by chance. Many works (Mora, 1987, 1988; Jannane et al., 1989; Pratt, 1999) show that reflection data is able to properly resolve only the high frequency information of the model with the single-scattering term. This indicates that for high frequency perturbations, residuals backprojected at once with multiple-scattering kernels can provide misleading estimates if not correctly handled.

Finally note that in this experiment, only δK_S^{est} should be nonzero. The fact that δK_B^{est} is also nonzero (Figure 6b) is a consequence of residual leakage since δp_s is generated by a singular-part perturbation only. We see that the leakage result contains almost the same information as the correct estimate for δK_S.

Experiment 2: lens-shaped background perturbation

In the next experiment, we only perturbed the background part of the model by introducing a lens-shaped background perturbation (see Figure 7). This yields a perturbation in both reference and scattered wavefields – see equation (6).

As we will see, this perturbation yields the most significant result of our set of experiments, namely that information on background perturbation can be extracted from the scattered-wavefield residual. In this experiment the full model perturbation is equal to the background perturbation only, i.e., $\delta K = \delta K_B$. This means that the true full residual δp^{true} is composed of a true scattered residual δp_s^{true} and a true reference residual δp_0^{true}. The expressions for the expected perturbation estimates do not simplify in this case. They are given by equation (7). The background perturbation estimate, δK_B^{est}, consists of two contributions, being the background perturbation estimate from the reference residual, $\delta K_{B,0}^{\text{est}}$ and the background perturbation estimate from the scattered residual, $\delta K_{B,s}^{\text{est}} = \sum_i \delta K_{B,i}^{\text{est}}$.

Figure 8 displays, from top to bottom, the full perturbation estimate, δK^{est}; and its two contributions, $\delta K_{B,0}^{\text{est}}$ and $\delta K_{B,s}^{\text{est}}$. The first thing to be noted is that the sum of $\delta K_{B,0}^{\text{est}}$ and $\delta K_{B,s}^{\text{est}}$ fairly accounts for the full estimate, δK^{est}. Doubtless, the estimate $\delta K_{B,0}^{\text{est}}$ from the reference residual (central part of Figure 8) is the one that represents the true medium perturbation best. The inversion done in this case is basically a transmission tomography, which is known to recover very well the low-frequency information specially when the target region is enclosed by both, sources and receivers (see,e.g., Pratt, 1999; Brenders and Pratt, 2007).

But the really important feature here is that $\delta K_{B,s}^{\text{est}}$ (bottom part of Figure 8) shows that a reasonable background perturbation estimate can be obtained with scattered-wavefield residuals. When transmission tomography fails (surface acquisition, for example) the background estimate obtained with the scattered

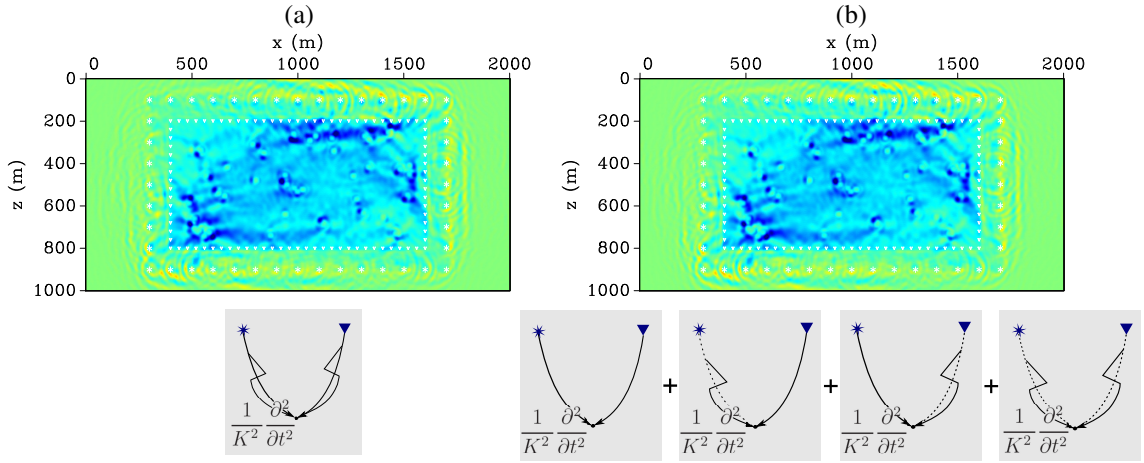

Figure 5: EXPERIMENT 1. Backprojection of the full (scattered) wavefield residual, $\delta p^{\text{true}} = \delta p_s^{\text{true}}$. Cartoons indicate the (sub)kernel used. (a) Bulk modulus perturbation estimate, δK^{est}, obtained with first equation of system (11) of Macedo et al. (2011). (b) Singular part of Bulk modulus perturbation estimate, δK_S^{est}, obtained with second equation of (10).

.

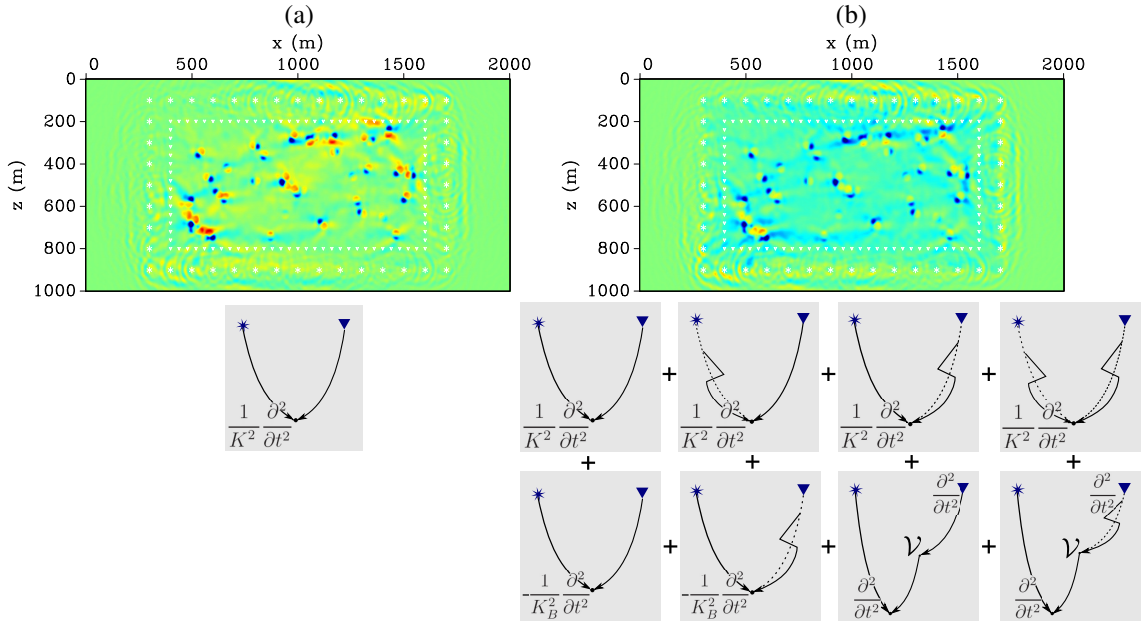

Figure 6: EXPERIMENT 1. (a) Singular part of Bulk modulus estimate, $\delta K_{S,0\mathcal{S}0}^{\text{est}}$, obtained with the single-scattering related kernel. Note that this estimates is very similar to the true perturbation observed in Figure 4. (b) Background bulk modulus estimate, $\delta K_{B,s}^{\text{est}}$, obtained with first equation of (10) (residual leakage).

residual stands as a possible option (see also experiment 3).

The most important estimate contributions to $\delta K_{B,s}^{\text{est}}$ are $\delta K_{B,0\mathcal{B}s}^{\text{est}}$ and $\delta K_{B,s\mathcal{B}0}^{\text{est}}$, displayed in Figure 9. Note that, except for the boundary regions close to sources and receivers, the terms $\delta K_{B,0\mathcal{B}s}^{\text{est}}$ and $\delta K_{B,s\mathcal{B}0}^{\text{est}}$ give the same estimate. Actually, any of these produces an image of almost the same quality as the sum of all contributions (cf. bottom part of Figure 8). None of the other contributions provides an image of similar quality.

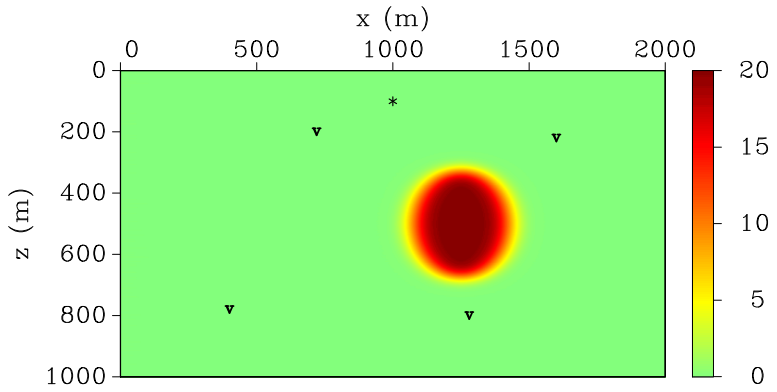

Figure 7: EXPERIMENT 2. Perturbation in the bulk modulus background model, δK_B. The scalebar shows, in percentage, the perturbation magnitude.

An analysis of the estimates from terms $0\mathcal{B}s$ and $s\mathcal{B}0$ from a single source-receiver pair (Figure 10) sheds further light on the symmetry highlighted in the previous paragraph. The source where the direct wavefield originates from is marked with a star. The receiver where the residual is observed and backpropagated from is cr530, marked by the triangle nearest to the bottom right corner. In Figure 10a, subkernel $U_{B,0\mathcal{B}s}$ is used to backproject residual and the singularities end up acting as receivers, i.e., the residuals seem to be backpropagated from there. On the other hand, in part b, subkernel $U_{B,s\mathcal{B}0}$ is used. There, the singularities act as sources, i.e., direct wavefields seem to originate from there. Complete coverage of sources and receivers around the area of interest completes the symmetry.

Experiment 3: Backprojecting residual from surface acquisition

This third experiment uses the same perturbed and unperturbed models as Experiment 2 (Figures 3(b) and 7), i.e., 60 random scatterers in a model with a lens-shaped background perturbation. The difference is the acquisition geometry: source and receivers are restricted to the top portion of the model, simulating a surface acquisition.

Figure 11 shows the backprojection results together with the acquisition geometry. As before, source and receivers are marked as white star and triangles, respectively. From top to bottom, the parts contain the undecomposed result δK^{est} backprojected in the full model, the estimate $\delta K^{\text{est}}_{B,0}$ obtained using only the reference-wavefield residual, and the estimate $\delta K^{\text{est}}_{B,s}$ using only the scattered-wavefield residual.

The restriction of the acquisition geometry affects the estimate from the full wavefield, δK^{est} (top part), which is not as good as the one in Figure 8. The estimate $\delta K^{\text{est}}_{B,0}$ (centre part) fails completely. The reason is that this estimate is based on transmission tomography, where only residuals of wavefields contribute that originate at one far side and were recorded at the other far side. In other words, for this acquisition geometry, there is not enough far offset to give a good estimate. Note, however, that estimate $\delta K^{\text{est}}_{B,s}$ (bottom part) provides much better quality.

In the same way as in the last experiment, we inspect the contributions $\delta K^{\text{est}}_{B,0\mathcal{B}s}$ and $\delta K^{\text{est}}_{B,s\mathcal{B}0}$ (Figure 12). Although at first sight, they are rather similar to each other, there are visible differences. They do not resemble each other as closely as the corresponding results in Figure 9 for Experiment 2. Also in difference to that experiment, these estimates no longer provide the best image of a single contribution. This is achieved by contribution $\delta K^{\text{est}}_{B,s\mathcal{B}s}$ (Figure 13a).

Finally, we compare this contribution to the one based on the conventional single-scattering based kernel, $\delta K^{\text{est}}_{B,0\mathcal{B}0}$ (Figure 13b). The latter is an example for a fast-varying sensitivity kernel in the sense of Zhu et al. (2009). According to this work, when dealing with reflection/scattered data, narrower offsets (or reflection angles) may lead to fast-varying sensitivity kernels, in opposition to slow-varying ones in large-offset acquisitions. Fast-varying sensitivity kernels cause slower convergence of the inversion procedure. On the other hand, the contribution $\delta K^{\text{est}}_{B,s\mathcal{B}s}$ from the strong multiple-scattering kernel is much smoother and closer to the full estimate δK^{est}. This is an important observation, because it allows to conclude that a

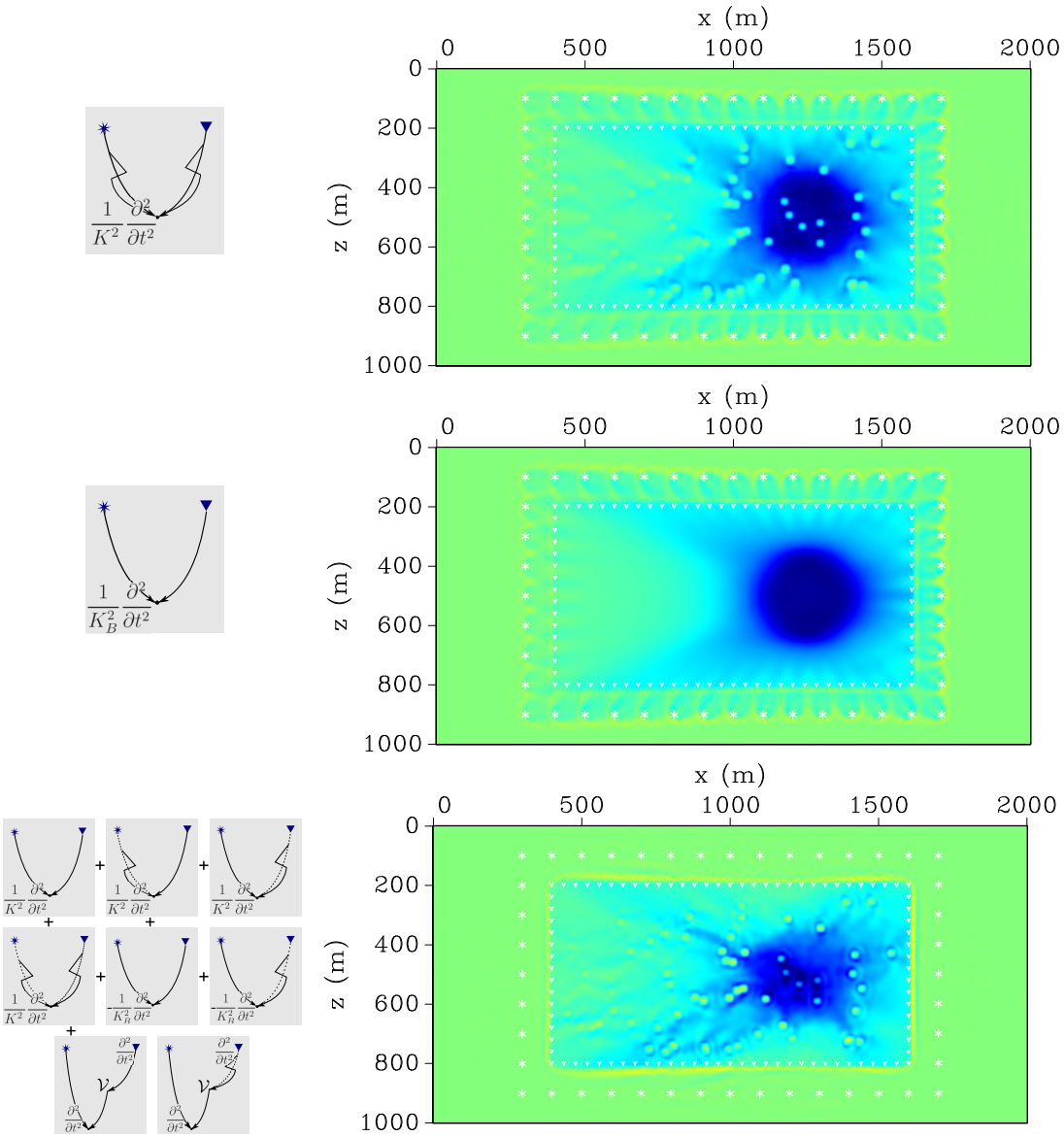

Figure 8: EXPERIMENT 2. Backprojection residuals. *Top:* The full residual, δp^{true} backprojected to get bulk modulus perturbation estimate, δK^{est}. *Centre:* reference residual, δp_0^{true}, to get background bulk modulus perturbation estimate, $\delta K_{B,0}^{\text{est}}$ (first equation of (7)). *Bottom:* scattered residual, δp_s^{true}, to get background bulk modulus perturbation estimate, $\delta K_{B,s}^{\text{est}}$ (first equation of (7)).

medium can "illuminate" itself by means of scatterers, so that the need for long offsets is reduced.

CONCLUSIONS

In continuation of the study presented in last year's WIT report (Macedo et al., 2011), we have shown that the separation of the sensitivity kernels into background and singular parts can add valuable information in full-waveform inversion. Estimates for both background perturbation and/or singular-part perturbation obtained with the subkernels' adjoints are components of the estimate obtained with the full kernel's adjoint.

Inversion based on adjoint methods can sometimes give better results than the inverse itself since adjoint operators tolerate imperfections in the data and do not demand that the data provide full information (Claerbout, 1985). On the other hand, insufficient cancellation of off-diagonal terms may result in residual

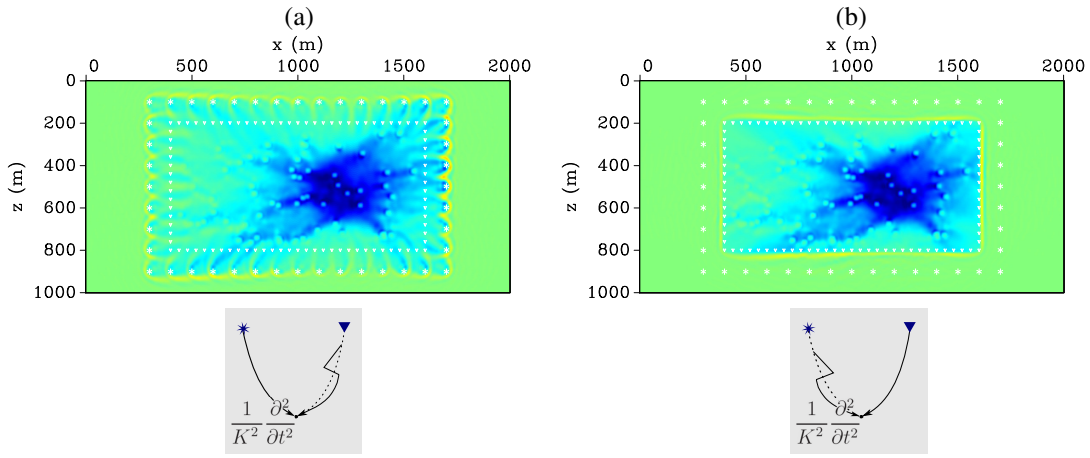

Figure 9: EXPERIMENT 2. Backprojection of scattered-wavefield residuals δp_S^{true}, using (a) subkernel $U_{B,0\mathcal{B}s}$, (b) subkernel $U_{B,s\mathcal{B}0}$. Note the very good match between both estimates except for the boundary region delimited by the receiver and source lines. It suggests a symmetry that can be wisely explored.

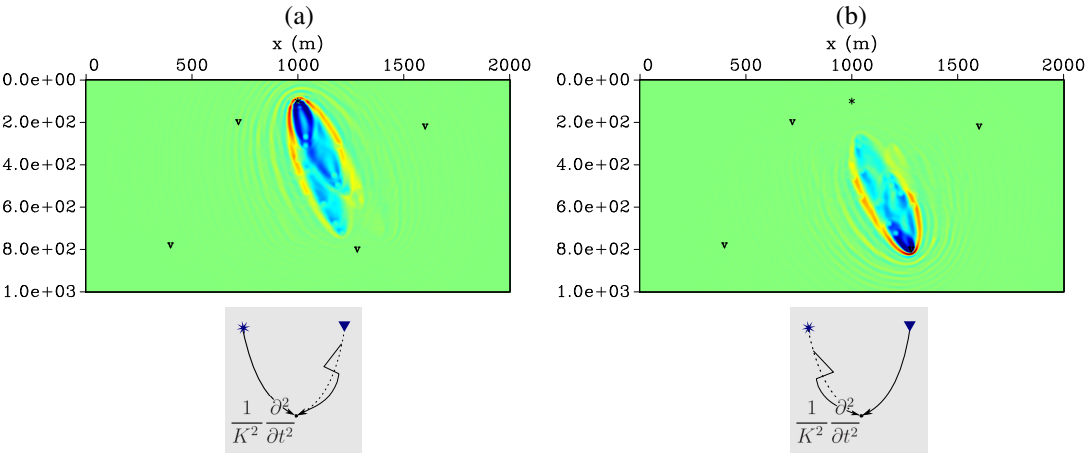

Figure 10: EXPERIMENT 2. Backprojection of scattered-wavefield residuals δp_S^{true} from point source (star) recorded at cr530. (a) Subkernel $U_{B,0\mathcal{B}s}$ used to backproject residual. Note that the singularities act as receivers. (b) Subkernel $U_{B,s\mathcal{B}0}$ used to backproject residual. Here, The singularities act as sources. This yields further insight on the symmetry in Figure 9.

leakage. This effect can be increased by the decomposition into subkernels.

We have also shown that multiple-scattering-based subkernels do a poor job when used to update the singular part of the model. The reason is that the scattered wavefield depends on the very same part of the model that is being updated. Actually the perturbation estimates end up being spread over the model as if they were background estimates.

On the bright side, our numerical experiments have shown the feasibility of our main claim: the decomposition into subkernels allows to backproject only the scattered-wavefield residuals so as to obtain reasonable background-model perturbation estimates.

In two experiments with background perturbation, we obtained the single best estimates with multiple-scattering subkernels. This was particularly important in experiment 3, which had a restricted acquisition geometry (reflection data, narrow offset). In this case, the multiple-scattering subkernels take advantage of medium self-illumination provided by the scattered wavefields. This suggests that FWI based on passive seismic might be possible, if scattered noise throughout medium is sufficient to achieve omnidirectional

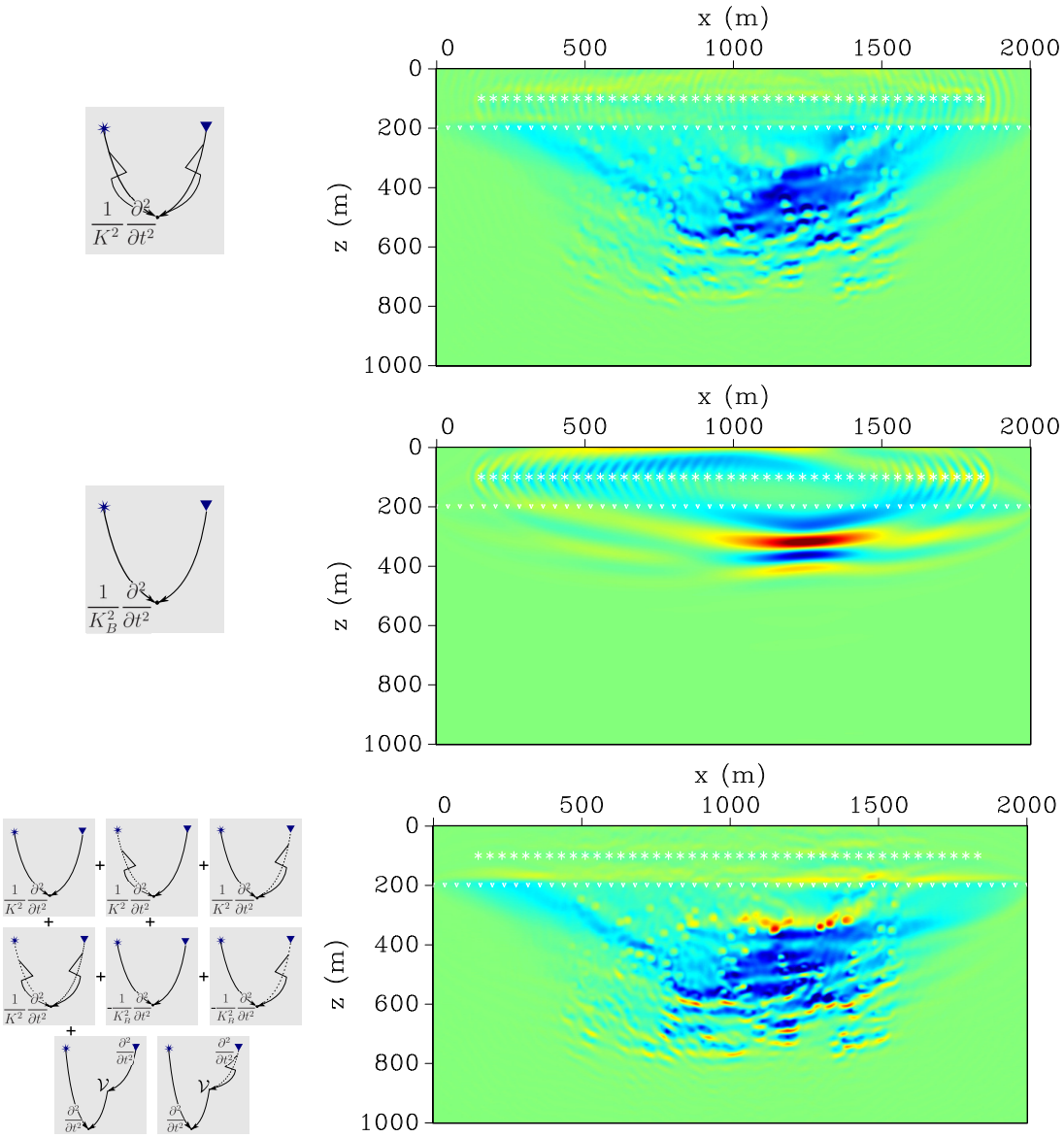

Figure 11: EXPERIMENT 3. Backprojection of residuals from "surface" receivers. *Top:* The full residual, δp^{true} backprojected to get bulk modulus perturbation estimate, δK^{est}. *Centre:* Reference residual, δp_0^{true}, to get background bulk modulus perturbation estimate, $\delta K_{B,0}^{\text{est}}$. *Bottom:* Scattered residual, δp_S^{true}, to get background bulk modulus perturbation estimate, $\delta K_{B,s}^{\text{est}}$.

illumination.

An important application of the subkernel decomposition, which is subject of ongoing research, is time-lapse seismics. In this framework, the baseline model is considered the unperturbed full model while the monitor is the perturbed one. The time-lapse change can be seen as background and/or a singular part perturbation. In this context, the separation of the reference and scattered wavefields becomes a simpler task.

Of course, a successful application of these concepts will rely on a good initial estimate for the singular part of the model. As pointed out in last year's report, a migrated image seismic image can be taken as a proxy for this singular part. Fleury and Snieder (2012) have recently employed this strategy with encouraging results.

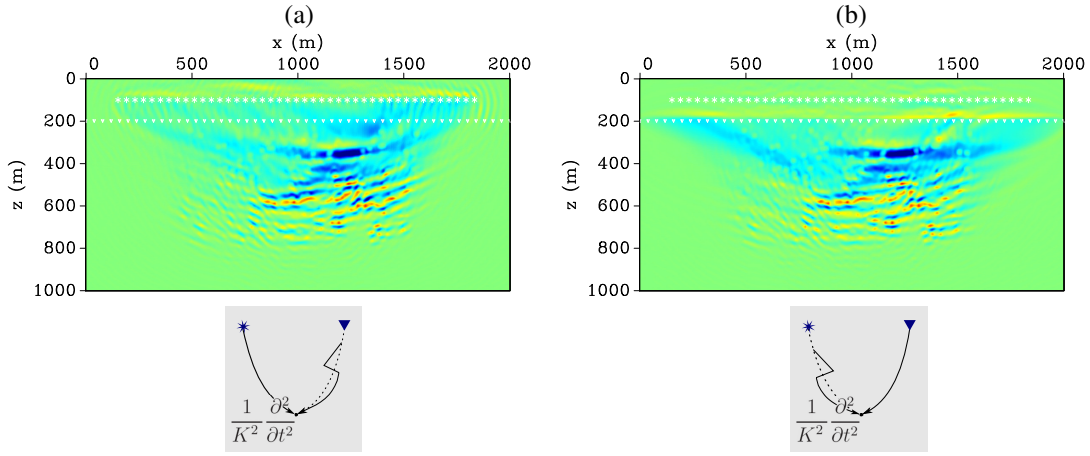

Figure 12: EXPERIMENT 6. Estimate contributions. (a) $\delta K^{\text{est}}_{B,0\mathcal{B}s}$. (b) $\delta K^{\text{est}}_{B,s\mathcal{B}0}$.

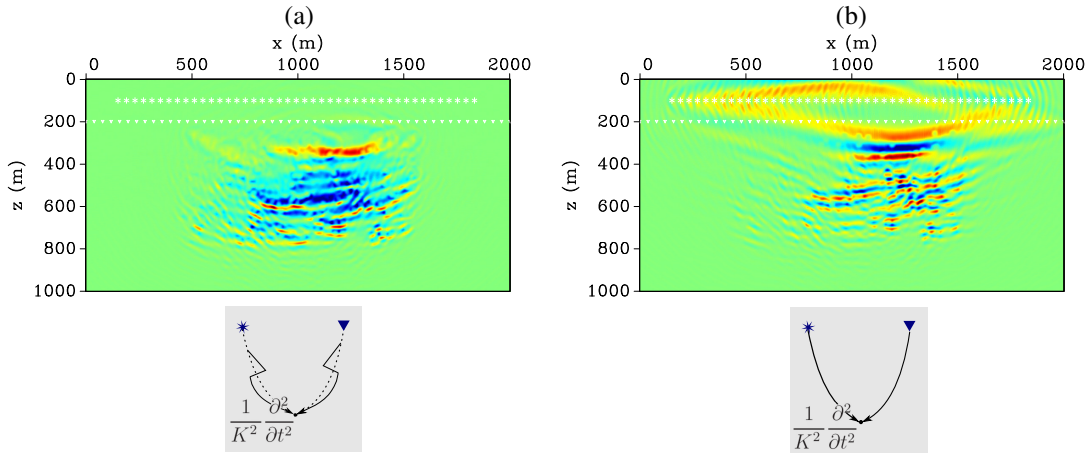

Figure 13: EXPERIMENT 6. Estimate contributions. (a) $\delta K^{\text{est}}_{B,0\mathcal{B}0}$. (b) $\delta K^{\text{est}}_{B,s\mathcal{B}s}$.

ACKNOWLEDGEMENTS

This work was kindly supported by the Brazilian National Research Council CNPq as well as Petrobras, Schlumberger, and the sponsors of the Wave Inversion Technology (WIT) Consortium.

REFERENCES

Brenders, A. J. and Pratt, R. G. (2007). Efficient waveform tomography for lithospheric imaging: implications for realistic, two-dimensional acquisition geometries and low-frequency data. *Geophysical Journal International*, 168(1):152–170.

Claerbout, J. F. (1985). *Imaging the Earth's Interior*. Blackwell Scientific Publications, Inc., Boston.

Crase, E., Pica, A., Noble, M., McDonald, J., and Tarantola, A. (1990). Robust elastic nonlinear waveform inversion: Application to real data. *Geophysics*, 55(5):527–538.

Fleury, C. and Snieder, R. (2012). Increasing Illumination and Sensitivity of Reverse-time Migration with Internal Multiples. *EAGE Tecnical Program Extended Abstracts*.

Jannane, M., Beydount, W., Crase, E., Cao, D., Koren, Z., Landa, E., Mendes, M., Pica, A., Noble, M.,

Roeth, G., Singh, S., Snieder, R., Tarantola, A., Trezeguet, D., and Xie, M. (1989). Wavelengths of earth structures that can be resolved from seismic reflection data. *Geophysics*, 54(7):906.

Macedo, D. L., Vasconcelos, I., and Schleicher, J. (2011). Scattering-based decomposition of sensitivity kernels for full waveform inversion. *Annual WIT Report*, 16:247–260.

Mora, P. (1987). Nonlinear two-dimensional elastic inversion of multioffset seismic data. *Geophysics*, 52(9):1211–1228.

Mora, P. (1988). Elastic wave-field inversion of reflection and transmission data. *Geophysics*, 53(6):750–759.

Pratt, R. G. (1999). Seismic waveform inversion in the frequency domain, Part 1: Theory and verification in a physical scale model. *Geophysics*, 64(3):888–901.

Snieder, R., Grêt, A., Douma, H., and Scales, J. (2002). Coda wave interferometry for estimating nonlinear behavior in seismic velocity. *Science*, 295:2253.

Tarantola, A. (1984). Inversion of seismic reflection data in the acoustic approximation. *Geophysics*, 49(8):1259–1266.

Tarantola, A. (1987). *Inverse problem theory: Methods for data fitting and model parameter estimation*. Elsevier Science Publ. Co., Inc.

Vigh, D., Starr, E. W., and Kapoor, J. (2009). Developing Earth models with full waveform inversion. *The Leading Edge*, pages 432–435.

Virieux, J. and Operto, S. (2009). An overview of full-waveform inversion in exploration geophysics. *Geophysics*, 74(6):WCC1.

Zhu, H., Luo, Y., Nissen-Meyer, T., Morency, C., and Tromp, J. (2009). Elastic imaging and time-lapse migration based on adjoint methods. *Geophysics*, 74(6):WCA167.